Enhanced Optical Property with Tunable Band Gap of Cross-linked PEDOT Copolymers via Oxidative Chemical Vapor Deposition

*Sunghwan Lee and Karen K. Gleason**

Highoptical transmittance conjugated-polymers with electrical conductivity are garnering much attention for the applications in organic optoelectronic devices including organic field-effect-transistors and solar cells. Polymers based on PEDOT are particularly promising candidates with high conductivity, uniform surface planarity and excellent ductility. In this work, homopolymer PEDOT deposited using oxidative chemical-vapor-deposition(oCVD) show the maximum conductivity of ≈3500 S/cm. However, their utility is limited due to the relatively low transmittance and abrupt decrease near the red edge in the visible regime. Here, the significantly improved optical properties achieved via tuning the bandgap of cross-linked PEDOT copolymers using oCVD, offering a single-step process for the synthesis and deposition of copolymer films, is reported. The cross-linking monomers of biphenyl or anthracene are simultaneously evaporated with EDOT monomer and an oxidant(FeCl3) during the deposition. Poly(anthracene-co-EDOT)[p(ANTH-co-EDOT)] shows the superior transmittance (≈93%) to homopolymer PEDOT (≈80%) and poly(biphenyl-co-EDOT)[p(BPH-co-EDOT)] (≈88%). Additionally, copolymers show no transmission decay in the red edge regime unlike homopolymer PEDOT that presents an abrupt transmission falloff. An improvement in optical transmittance is in agreement with an increase in bandgap of materials (p(ANTH-co-EDOT), ≈2.3eV vs PEDOT, ≈1.8 eV). oCVD-processed bandgap-tunable PEDOT copolymers with enhanced transmittance may, therefore, have applications in organic optoelectronic devices that require high optical transparency.

1. Introduction

The discovery of electrical conductivity in π-conjugated polymers[1] has sparked considerable activity in both academic and industry electronics research to develop materials that are highly conductive, electrically stable, easily processible and relatively simple to produce at low cost. Of the π-conjugated polymers with electrical conductivity, many researchers have been attracted by polymers based-on polyacetylene,[2,3] polypyrrole,[4] polythiophene,[2,5] polyphenylene,[2] polyphenylene-vinylene,[2] polyaniline[6] and poly(3,4-ethylenedioxythiophene) (PEDOT),[3,7] and their derivatives. **Table 1** summarizes[2–8] the characteristics of these polymers: the band gap, electrical conductivity, dopant counterion, and chemical structure. This class of materials has been extensively implemented as electrodes, electrical conductors (e.g., charge carrier transport layers) and semiconducting active layers in many organic electronic and optoelectronic devices that include light-emitting diodes,[9] field effect transistors[10] and photovoltaic cells.[11–13] These devices have successfully demonstrated high device performance comparable to classical Si- or oxide-based technologies. Polymers based on PEDOT[3,14] are of particular interest due to their high electrical conductivity, mechanical flexibility, as well as their stability relative to other conjugated polymers.

Oxidative chemical vapor deposition (oCVD) offers a facile approach to synthesize and deposit conjugated polymers irrespective of polymer solubility or the properties of the substrate material. The oCVD method has the merits of good film uniformity[7,15] over the large areas, high electrical conductivity,[15] conformal coating on non-planar[12,13] (e.g., textiles and papers) and patterned[16,17] (e.g., trench) substrates, and relatively low process temperature[15,17] (25–150 °C). Previously, we reported on the oCVD synthesis of conjugated homopolymer thin films of the doped conducting polymer PEDOT[15,17] with systematically tunable band gap over ≈0.3 eV[14] and excellent adhesion to the substrate through grafting.[18] The oCVD platform has been demonstrated for the dedoped semiconducting homopolymers polythiophene,[19,20] polyisothianaphthene,[21] and polyselenophene.[22] The oCVD synthesis method has also achieved copolymers from thiophene-3-acetic acid with EDOT[23] and with pyrrole.[24] Additionally, 3-thiopheneethanol (3-TE) has been oCVD copolymerized with EDOT.[25] The oCVD films find application including transparent conductors for electrodes[13] and carrier transport layers,[26] sensors[23,25,27] and electrochromic devices.[28]

Dr. S. Lee, Prof. K. K. Gleason
Department of Chemical Engineering
Massachusetts Institute of Technology
Cambridge, MA 02139, USA
E-mail: kkg@mit.edu

DOI: 10.1002/adfm.201402924

Table 1. Electrical properties of the band gap (E_g) and conductivity (σ) for the major conjugated conducting polymers with structure and selected dopant counterions.

Polymer	Structure	E_g [eV]	Dopant counterion	σ (S cm^{-1})	Ref.
Polyacetylene	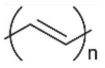	≈1.5	I^-, Br^-, AsF_6^-, $(As_2F_{10})^{2-}$, Li^+, Na^+	~10^3–10^4	[2,3]
Polypyrrole	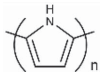	≈3.1	BF_4^-, ClO_4^-, *TsO^-	~10^2–10^3	[4]
Polythiophene	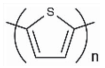	≈2.0	BF_4^-, ClO_4^-, $FeCl_4^-$, *TsO^-	~10–10^3	[2,5]
Polyphenylene	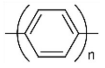	≈3.0	AsF_6^-, $(As_2F_{10})^{2-}$, Li^+, K^+	≈5×10^2	[2]
Polyphenylene-vinylene	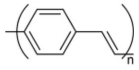	≈2.5	AsF_6^-, $(As_2F_{10})^{2-}$	~10–10^3	[2]
Polyaniline	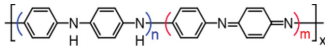	≈3.2	Cl^-	~10–10^2	[6]
PEDOT	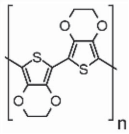	≈1.5–2.0	$FeCl_4^-$, Cl^-, Br^-, I^-, **PSS^-	~10–10^3	[3,7,8]

*poly(toluenesulfonic acid) counterion (tosylate)
**poly(styrenesulfonic acid) (PSS) counterion

For the applications in organic optoelectronic and display devices such as solar cells, light emitting diodes and transparent thin film transistors (TFTs), high optical transparency must be achieved in the visible wavelength regime of light along with the electrical conductivity. Homopolymer PEDOT is most widely used transparent conductor in organic device applications. As a figure of merit, the percent optical transmittance at λ = 550 nm from films thicker than 50 nm will be compared. Vapor-phase polymerized PEDOT:poly(styrenesulfonic acid) (PSS) show ≈80% (≈60 nm-thick),[29,30] solution processed PEDOT:PSS display <≈75% (≈60 nm-thick)[30] and oCVD PEDOT are ≈80% (≈50 nm-thick).[28] Comparing to other materials: sputtered indium tin oxide (ITO) shows >80%,[31] metal nanogrids have ~80%,[32] single-wall carbon nanotubes display ≈70%,[33] CVD-grown graphene have >85%,[34] and graphene oxide shows ≈75%.[35] In the present study, we report on the significantly enhanced optical transmittance (up to >93% in ≈55 nm-thick film) of oCVD PEDOT copolymer films achieved by the incorporation of crosslinking monomers of anthracene and biphenyl associated with tuning the energy band gap to higher values. oCVD copolymer PEDOT films along with homopolymer film were systematically characterized with UV–Vis–NIR spectroscopy to investigate the optical transmittance and band gap, X-ray diffraction to determine amorphous/crystalline structure of the films, and atomic force microscopy to obtain the surface topographic images with roughness. Fourier transform infrared, Raman and X-ray photoemission spectra were collected in order to compare the chemical bonds and doping level of homo- and copolymer PEDOT films deposited using oCVD.

2. Results and Discussion

Oxidative chemical vapor deposition (oCVD) enables the synthesis, deposition, and doping of conjugated polymers simultaneously in a single step. In the present study, band gap-tuned copolymers of PEDOT were successfully deposited with cross-linking monomers of anthracene or biphenyl. **Figure 1**(a) shows images of the resulting films of the oCVD copolymers of poly(anthracene-co-EDOT) [p(ANTH-co-EDOT)] and poly(biphenyl-co-EDOT [p(BPH-co-EDOT)] on glass substrates with a reference of typical oCVD homopolymer PEDOT. The p(ANTH-co-EDOT) films deposited below the temperatures of 150 °C are readily detached from the glass substrates as displayed for the film prepared at T_s = 120 °C, while the films deposited at substrate temperatures higher than 150 °C, no film detach from the substrates is observed in p(ANTH-co-EDOT) as presented in Figure 1a. The homopolymer PEDOT and p(BPH-co-EDOT) films are well grown regardless of the substrate temperatures. Figure 1b,c show the optical properties of the transmittance and absorption spectra, respectively which were obtained using UV–Vis–NIR spectroscopy. The percent transmittance were measured on approximately 55 nm-thick homopolymer and copolymer PEDOT films in the visible regime ranging from 300 to 800 nm. Overall transmittance of PEDOT copolymers in Figure 1b was substantially improved over that of the homopolymer PEDOT, in particular toward the red edge regime where regular PEDOT shows an abrupt decrease in transmittance at the wavelength above ≈450 nm while copolymer films maintain excellent transmittance of higher than ≈88%.

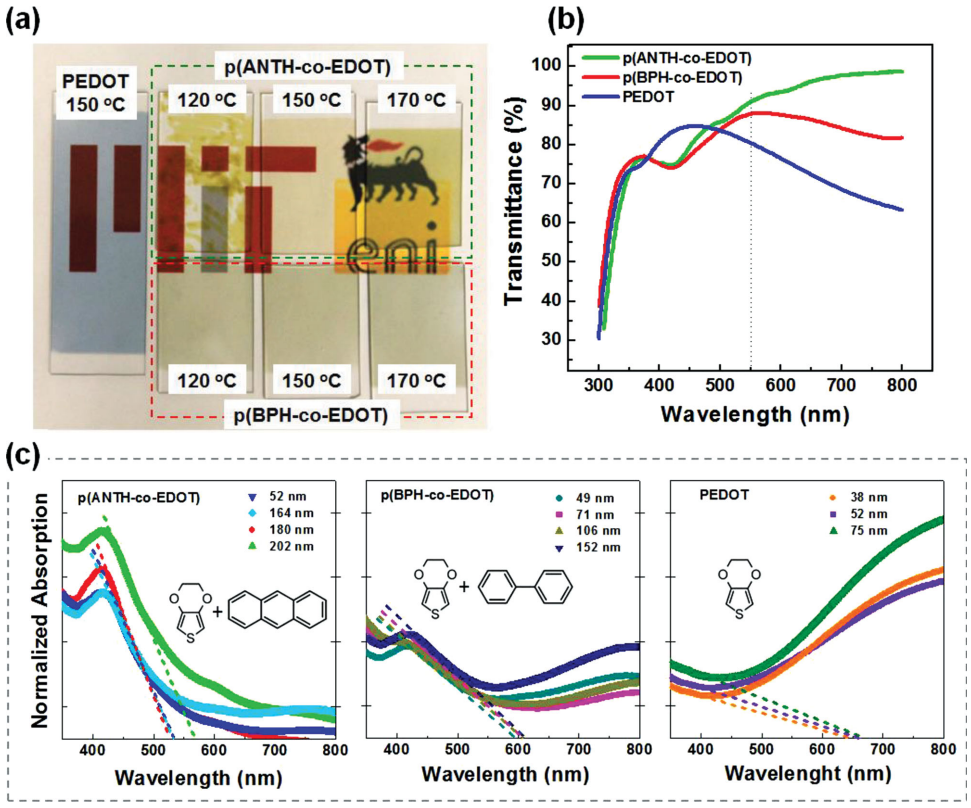

Figure 1. Optical properties of homopolymer and copolymer PEDOT films. a) Photographs of p(ANTH-co-EDOT) and p(BPH-co-EDOT) copolymers with typical homopolymer PEDOT deposited on 25 mm × 75 mm glass slides. b) Optical transmission spectra from ≈55 nm-thick samples investigated in the visible regime from 300 to 800 nm. The dotted line indicates the standard light wavelength of 550 nm. c) Normalized absorption spectra of oCVD polymers as a function of film thickness. Each inset shows the monomer(s) used.

The p(ANTH-co-EDOT) copolymer shows the highest transmittance of 93% among the films at the typical wavelength of 550 nm, and at higher wavelength region the transmittance increases unlike homopolymer PEDOT and p(BPH-co-EDOT) films. The absorption spectra shown in Figure 1c and the corresponded band gap clearly account for the enhancement in optical transmittance of PEDOT copolymers compared to the homopolymer films. The optical band gap (E_g) is determined from the equation of $E_g = hc/\lambda_{ab}$ that relates the E_g to the Planck constant (h), the speed of light (c), and the absorption edge wavelength (λ_{ab}).[36] From largest to smallest, the determined band gap values are p(ANTH-co-EDOT) (2.3 ± 0.06 eV), p(BPH-co-EDOT) (2.1 ± 0.03 eV), and PEDOT (≈1.8 ± 0.04 eV). Note that the measured band gap of oCVD polymers is similar to reported values of PEDOT (≈1.6 eV, solution-processed)[37] and PEDOT:PSS, p(BPH-co-EDOT) (≈2.3 eV)[38] and p(ANTH-co-EDOT) (≈2.3 eV, electrochemically copolymerized).[39] The incorporation of crosslinking monomers leads to an increase in band gap which is likely attributed to the incorporation of wider band gap materials of anthracene and biphenyl into smaller band gap PEDOT. The band gap of cross-linking monomers of anthracene and biphenyl utilized in the present study is found from the literature[40] as approximately 3.8 eV for both monomers, which support the suggestion that inserting these crosslinking monomers into copolymerization process increases the band gap compared to the homopolymer PEDOT. An increase in band gap, consequently, results in the improvement of the optical transmittance shown in Figure 1b as generally expected that wider band gap materials are more transparent due to less undesirable absorption than smaller band gap semiconductors.[41] This is consistent with the results of absorption spectra in Figure 1c that show that among the samples in the thickness ≈55 nm, p(ANTH-co-EDOT) film with the highest band gap is absorbing the least visible light at the wavelength of 550 nm and above.

oCVD polymers offer significant improvements in process and performance over conventional solution-processed polymers. Optical properties of visible transmittance/absorption and band gaps of oCVD homo- and co-polymer PEDOT films in Figure 1 describe the facile route to tailor the band gap of PEDOT-based polymers by simply incorporating cross-linking monomers into EDOT during the deposition. Since the band gap, as the specific characteristic of the materials, accounts for many electrical and optical properties of materials, the ability to tune the band gap is substantially promising in the semiconductor device applications. The work function of the materials, which is defined as the minimum energy required for an electron to escape from the Fermi level (E_F) into a vacuum, is of great important in multi-layered devices such as thin film transistors and thin film solar cells in order to align the energy levels among dissimilar layers to limit the barrier height for the appropriate charge carrier transport. oCVD can also tune the E_F

by varying the doping level in the resulting films throughout the insertion of cross-linking monomers and consequently, the work function of the materials is likely, at least in part, to be engineered using the oCVD technique. In addition, since physical properties of thin films such as sheet resistance and surface scattering, consequently charge transport often depend on the thickness, straightforward control of the film thickness during oCVD process which is easily managed by the deposition time provides great process simplicity compared to solution-phase process for the optoelectronic device applications. Other process-wise advantages of the use of oCVD compared to solution phase process include: solvent-free process which enables synthesizing and depositing insoluble polymers such as PEDOT, polythiophene, and their derivatives; no dewetting defects which are often seen in solution-processed polymers and causes significant non-uniformity in conductivity and film morphology; simple patterning in situ shadow masking. Previous studies show also superior substrate compatibility with flexible polymer (e.g., PET), Styrofoam and a variety of papers (e.g., tissue, wax and magazine papers) and excellent conformality over complex and patterned structures such as trench wafers and textiles.

The measured electrical conductivity oCVD-processed homopolymer PEDOT, and copolymer PEDOT having incorporated anthracene and biphenyl is presented in **Figure 2**. Previously, thicker homopolymer oCVD PEDOT were observed to have reduced conductivity, hypothesized to be due to the inability to completely remove residual $FeCl_3$ from the thicker films and/or increasing disordered polymer chain alignment with increasing thickness.[42] The similar thickness effect on the conductivity is observed for p(BPH-co-EDOT); on the contrary, no dependence on thickness is seen in p(ANTH-co-EDOT) films. The absence of a thickness effect in p(ANTH-co-EDOT) is likely attributed to very low initial doping level. All the homopolymer PEDOT films <50 nm in thickness show very high conductivity of >2000 S cm^{-1} (Figure 2). The highest conductivity of 3572 S cm^{-1} from 25 nm-thick homopolymer PEDOT film is obtained with a low deposition rate <0.5 nm min^{-1} in the present study. Achieved high conductivity using oCVD process is greatly promising for the use of homopolymer PEDOT as transparent electrode applications. The electrical conductivity of the copolymers of PEDOT is in the range of ≈20–35 S cm^{-1} for p(BPH-co-EDOT) and ≈0.1–0.7 S cm^{-1} for p(ANTH-co-EDOT) films. Since the band gap is the energy required to add or subtract a charge carrier to the material system, the higher band gap for copolymers yields the lower intrinsic conductivity. Doping level, additional factor to contribute the electrical conductivity, will be discussed in later sections. These PEDOT copolymers exhibiting the electrical conductivity to a semiconducting degree with excellent optical transmittance of ~90% in the visible regime may be of great candidates as active layers in organic optoelectronic devices such as transparent thin film transistor channel and photovoltaic buffer materials.

The Raman spectra for the homopolymer and copolymer PEDOT films are shown in **Figure 3**a. Full spectra (upper figure) ranging wavenumbers from 150 to 2300 cm^{-1} of all oCVD PEDOT films present strong Raman bands near 435, 576, 985, and 1420 (very strong) cm^{-1} along with medium and

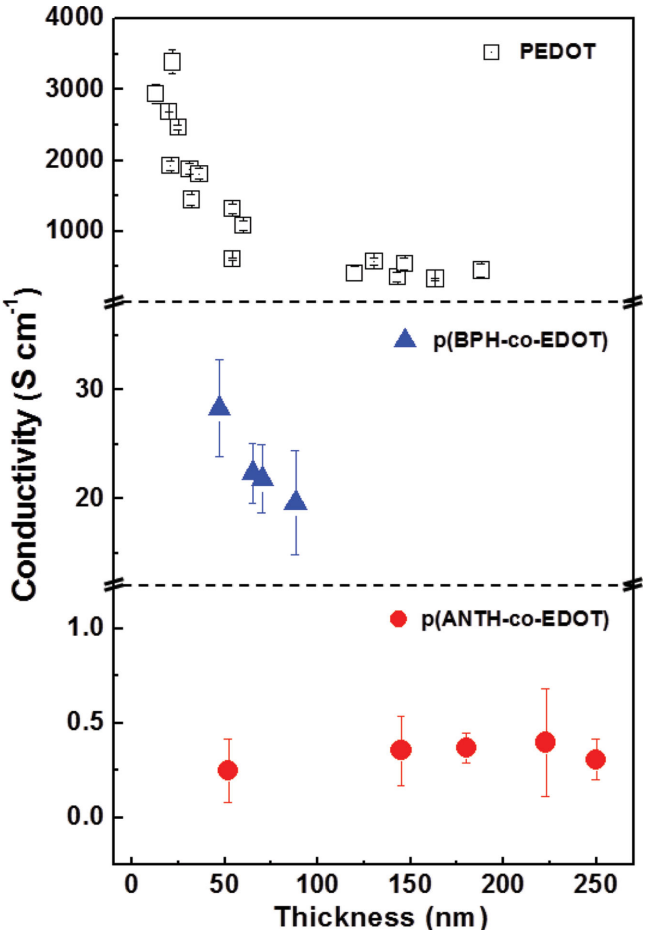

Figure 2. Electrical conductivity of oCVD homopolymer and copolymer PEDOT films as a function of film thickness.

weak bands around 206, 317, 524, 696, 853, 1094, 1262 cm^{-1}. In the expanded spectra (1280–1550 cm^{-1}, lower figure), a strong peak at approximately 1413 cm^{-1} for homopolymer PEDOT is the characteristic peak of symmetric $C_\alpha = C_\beta$ stretching[20,43,44] with a shoulder at ~1363 cm^{-1} attributed to $C_\beta = C_\beta$ stretching[44,45] peak that are typically observed in PEDOT films. For the copolymer PEDOT films, no significant shifts were observed in $C_\beta = C_\beta$ peak at ≈1363 cm^{-1} compared to homopolymer PEDOT. The symmetric $C_\alpha = C_\beta$ peaks of copolymers, however, were shifted to ≈1438 cm^{-1} for p(BPH-co-EDOT) and to ≈1441 cm^{-1} for p(ANTH-co-EDOT) films. Ouyang et al.[43] and Im et al.[20] reported that the $C_\alpha = C_\beta$ peak at lower wavenumber of ≈1410 cm^{-1} is due to doped quinoidal (lower scheme in Figure 3b) vibration contributing high conductivity while the peak of copolymers at higher wavenumber of ≈1440 cm^{-1} is attributed to undoped benzoidal (upper scheme in Figure 3b) vibration that yields relatively low conductivity. Thus, the upshift of the $C_\alpha = C_\beta$ peak observed in copolymer PEDOT films from 1410 to 1440 cm^{-1} indicates that the nature of conjugation is altered from doped quinoid (longer conjugation) and undoped benzoid (shorter conjugation), consistent with the observed decrease in conductivity with copolymerization.

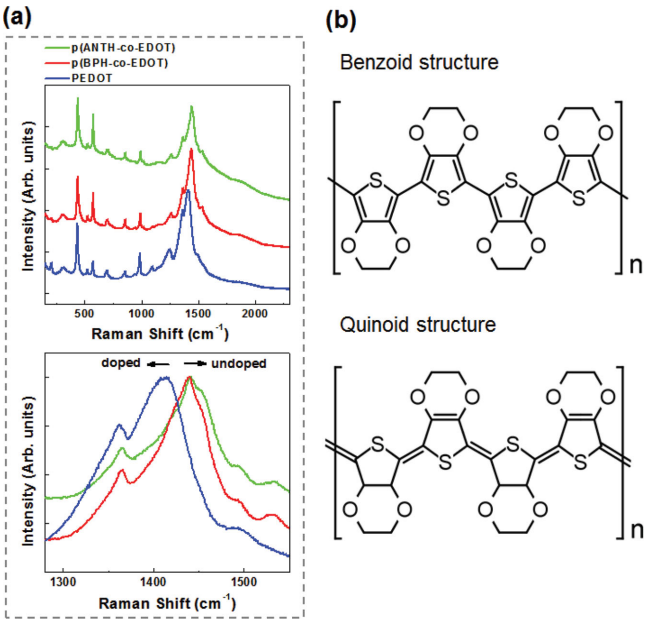

Figure 3. a) Full (upper) and expanded (lower) Raman spectra of oCVD homo- and copolymer PEDOT films showing upshift of the symmetric $C_\alpha = C_\beta$ stretching peak in copolymers which indicates shorter conjugation. b) Two types of conjugation: undoped benzoid (upper) and doped quinoid (lower) structures that account for the difference in Raman spectra.

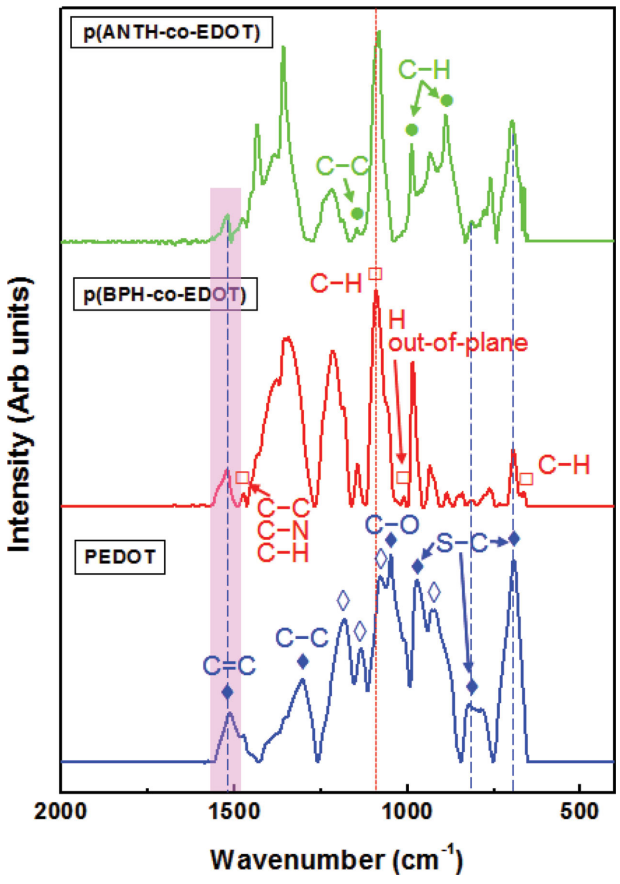

Figure 4. FTIR absorption spectra collected from oCVD polymers of homopolymer PEDOT (♦ and ◊), copolymers of p(BPH-co-EDOT) and p(ANTH-co-EDOT). The unlabeled peaks (◊) in homopolymer PEDOT result from the ethylendioxy group. The characteristic features of biphenyl and anthracene are assigned with □ and ●, respectively.

Figure 4 presents the spectra of the Fourier transform infrared (FTIR) spectroscopy. The obtained FTIR spectrum of homopolymer PEDOT shows similar primary features as previously reported PEDOT(:PSS) films[20,46–48] and each copolymer FTIR measurement shows both the characteristic peaks of PEDOT and each crosslinker, which verifies, at least in part, the resulting copolymer films are crosslinked by the incorporation of crosslinking monomers of anthracene and biphenyl. Homopolymer PEDOT film (♦ indexed and ◊ un-indexed in the bottom plot of Figure 4) exhibits peaks at approximately 1520 and 1340 cm^{-1} are attributed to stretching modes of C = C and C–C bonds in the thiophene ring,[47,48] respectively. The vibrations of C–S bond[47,48] in the polymerized PEDOT chains are observed at ~971, 830 and 692 cm^{-1}. The bands at ≈1184, 1132, and 1093 cm^{-1} correspond to the C-O-C bond stretching modes of the ethylenedioxy group,[47,48] and the band near 920 cm^{-1} results from the deformation mode of the ethylenedioxy ring.[48] The vibration at ≈1049 cm^{-1} is likely attributed to the C–O bond stretch.[47] The FTIR result of the p(BPH-co-EDOT) (middle in Figure 4) shows the characteristic vibration modes of the biphenyl[49] (□) as well as homopolymer PEDOT; the vibrations of the C–C/C–N stretching at ≈1473 cm^{-1}, C–H bending at ≈1473, 1091 and 661 cm^{-1}, and out-of-plane motion of H atoms at ≈1010 cm^{-1} due to the displacement perpendicular to the plane of the appropriate ring are detected as typically seen in biphenyl ($C_{12}H_{10}$).[49] The C = C (1520 cm^{-1}) and C–S (830 and 692 cm^{-1}) bands are also observed at the identical wavenumbers as shown in homopolymer PEDOT film. The p(ANTH-co-EDOT) FTIR spectrum presented in the top of Figure 4 includes the vibrations of C–C stretching at approximately 1145 cm^{-1} and out-of-plane C–H bending at ≈987 and 889 cm^{-1} of typical anthracene (●, $C_{14}H_{10}$)[50] along with the C = C stretching (1520 cm^{-1}) and C–S (830 and 692 cm^{-1}) bands of the homopolymer PEDOT as observed in p(BPH-co-EDOT).

Despite the difficulty of the detailed quantitative analysis due to the broadness and peak overlaps/shifts and limited literatures to compare with because of the novelty of the present study, the resulting FTIR absorption spectra clearly show that the peak intensity at ≈1520 cm^{-1} correlating C = C stretch decreases with the incorporation of crosslinking monomers. The highest C = C stretch is observed from homopolymer PEDOT, intermediate intensity from p(BPH-co-EDOT) and the lowest from p(ANTH-co-EDOT) films. Since a decrease in C = C stretch at ≈1520 cm^{-1} indicates short conjugation length[20] describing less doping in copolymer films than that of homopolymer PEDOT, the FTIR results are in consistence with the Raman spectra shown in Figure 3. The broadness of the FTIR peaks at the wavelength between 1450 and 700 cm^{-1} is also attributed to the doping level since the infrared absorption increases with increasing carriers within the band gap and/or near the band edge. Consequently, broader peaks refer to higher doping level and longer conjugation in conducting polymers. In Figure 4, absorption peaks from copolymer PEDOT

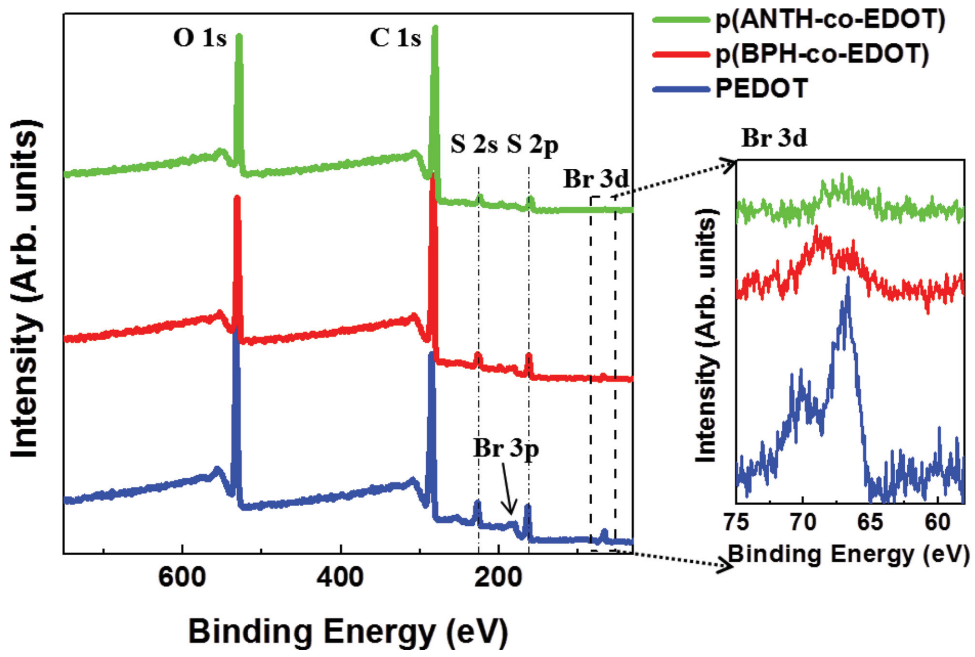

Figure 5. XPS full spectra (left) and focused high resolution scans of the Br 3d core-level (right) surveyed from oCVD homopolymer and copolymer PEDOT films.

films are relatively narrow compared to those of homopolymer PEDOT that is ascribed to less doping in copolymers.

X-ray photoemission spectroscopy (XPS) survey scans were made on the samples of homopolymer and copolymer PEDOT films, and are presented in **Figure 5**. The obtained XPS spectra are similar to each other showing strong intensity of O 1s and C 1s peaks. However, clear differences are observed among samples for the intensity of the sulfur- and bromine-related chemical bonding environments. Copolymers show smaller intensity of the peaks of S 2s, 2p than those of homopolymer PEDOT, which is attributed to less EDOT density in copolymerized films. Since it is widely accepted for PEDOT oxidative polymerization[46,51] that S in EDOT monomer acts as a charge carrier (hole) generator by the oxidizing agent ($FeCl_3$ in this study), smaller intensity of S 2s and 2p in copolymers indicates less doping in copolymer films than in homopolymer PEDOT film. The Br 3d core-level high resolution XPS spectra are also given at the right side of the full spectra and show that the intensity of copolymers is much weaker than the homopolymer PEDOT intensity. HBr acid rinsing is known to effectively remove residual $FeCl_3$ and dope PEDOT additionally with the new dopant of bromine anion.[7] Consequently, smaller intensity of Br 3d peak in copolymers indicates less additional doping by HBr rinsing. These XPS analyses indicate a higher doping level for homopolymer than for copolymer PEDOT films, which is also in good agreement with the previously discussed Raman and FTIR results in Figure 3 and 4.

The surface topographic images were obtained using non-contact atomic force microscopy (AFM) to examine microstructures and surface roughness of oCVD processed homo- and copolymer PEDOT films. **Figure 6**a–c represent AFM height-mode images of p(ANTH-co-EDOT) (thickness of ≈50, 150, 300 nm), p(BPH-co-EDOT) (≈50, 110, 155 nm) and homopolymer PEDOT (≈35, 50, 80 nm) films, respectively. Copolymer films (Figure 6a,b) seem to initially grow in granular morphologies as shown in relatively thin films, then spiral rod and vertically aligned sheet type in thicker films. However, homopolymer PEDOT (Figure 6c) is grown more laterally networked than copolymers, and no significant difference is observed with increasing thickness. The root mean square (RMS) surface roughness of oCVD polymer films in different thicknesses is summarized in **Table 2**. Of samples of the similar thickness of approximately 50 nm, copolymer films show higher roughness than the homopolymer film possibly due to the forming nature (rod or vertical sheet type) of the copolymers.

Figure 7 shows Bragg-Brentano scan X-ray diffraction (XRD) spectra from the ≈50 nm-thick oCVD films on glass substrates. The homopolymer PEDOT sample shows peaks associated with polycrystalline (100) (strong) and (101) iron hydroxide ($Fe(OH)_2$) at diffraction angle, 2θ of ≈31° and ≈37°, respectively along with other weak polycrystalline peaks of (200) and (020) iron oxide hydroxide (FeOOH) at $2\theta \approx 36°$ and ≈40°. In XPS survey scans shown in Figure 5, no significant Fe 2p related peaks are observed in HBr-rinsed homopolymer PEDOT films. However, since the XPS analysis is typically performed within the ≈10 nm depth profile from the surface, Fe-related components are expected to be present inside the film further from the surface in both HBr- and MeOH-rinsed samples as shown in XRD patterns. Note that the X-ray penetration depth of the typical θ-2θ XRD scan analysis is larger than 50 nm. Therefore, the post-process acid rinsing is likely to be effective in the thickness range of approximately 10–20 nm from the surface. In addition, our recent stability study[42] shows that $FeCl_4^-$, a dopant counter anion in PEDOT reacts with water and oxygen

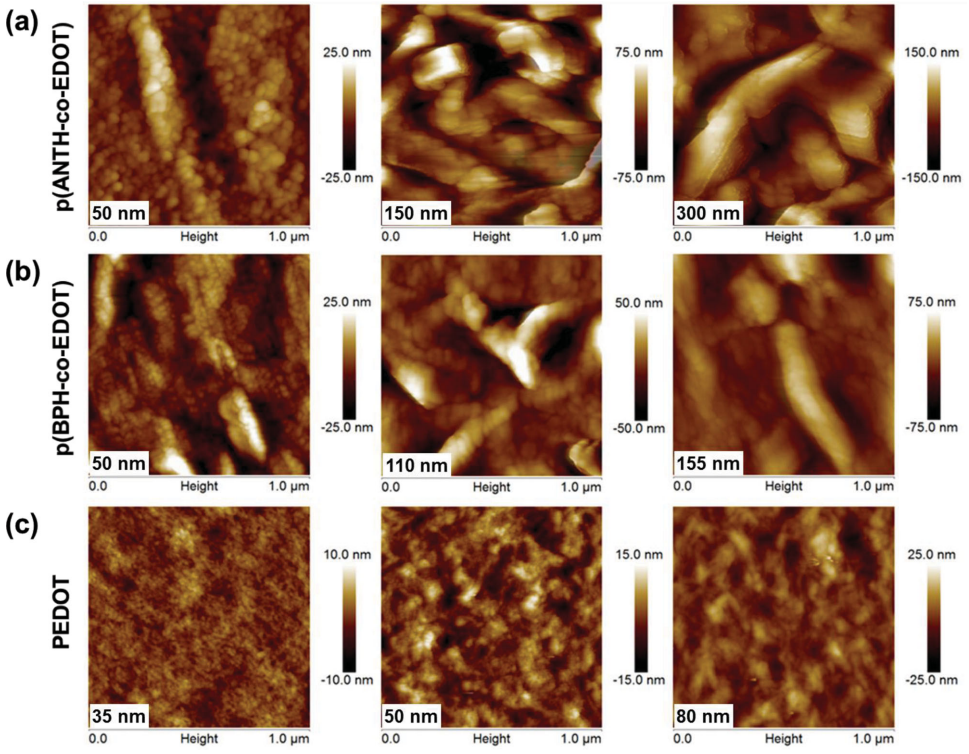

Figure 6. AFM surface topographic images obtained via non-contact height mode from oCVD films of a) p(ANTH-co-EDOT), b) p(BPH-co-EDOT) copolymers, and c) homopolymer PEDOT in different thickness.

and produce $Fe(OH)_2$ which is responsible for the Fe-related peaks shown in the XRD spectrum of heavily doped homopolymer PEDOT. XRD patterns of p(ANTH-co-EDOT) and p(BPH-co-EDOT) copolymers are not showing any indicative crystallographic intensity of the peaks. Note, thereafter, that the rod and vertical sheet-like copolymers shown in the AFM topographic images in Figure 6a,b were deposited in amorphous state using oCVD. Similar broad peaks located at 2θ from ≈8° to ≈11° are attributed to amorphous state PEDOT in homo- and copolymer films. Another amorphous peak in the range of approximately $15° < 2\theta < 35°$ is observed due to the glass substrate. In general, films in amorphous phase are more ductile than crystalline state films whose soft characteristic is promising for the implementation in future flexible and foldable optoelectronic devices. The doping level of the films can also be partly accounted for by the Fe-related peaks in the diffraction patterns since the Fe species in the crystalline phases of $Fe(OH)_2$ and FeOOH, in part, originate from the dopant anion of $FeCl_4^-$,[42] which suggests that PEDOT copolymers were less doped by $FeCl_3$ (oxidative doping agent) than homopolymer film. The doping level analysis, here, using XRD data is in agreement with previously discussed Raman, FTIR and XPS measurements.

The need in a given application relies on a variety of properties. In many cases, it is not purely conductivity. For various device applications such as photovoltaics (active/buffer layer), sensors, and field effect transistors (channel), the required property is the product of transparency and conductivity. The systematic studies in this report show a way to improve the transparency. Further efforts to improve the electrical conductivity are still valuable for transparent electrode applications. Additional doping through post iodine-vapor treatment, maximizing doping level using pulsed-monomer-delivery with continuous flow of doping agent, and/or enhancing carrier transport through defect passivation and chain end-group control would potentially enhance the electrical conductivity.

3. Conclusions

In this report, the ability to tune the band gap of the copolymer films is successfully demonstrated using oxidative CVD

Table 2. Surface RMS roughness of oCVD homo- and copolymer PEDOT films measured using non-contact height mode AFM.

oCVD polymers	p(ANTH-co-EDOT)			p(BPH-co-EDOT)			PEDOT		
Thickness [nm]	50	150	300	50	110	155	35	50	80
RMS roughness [nm]	7.04	22.6	26.5	6.94	14.1	16.2	1.86	2.16	3.14

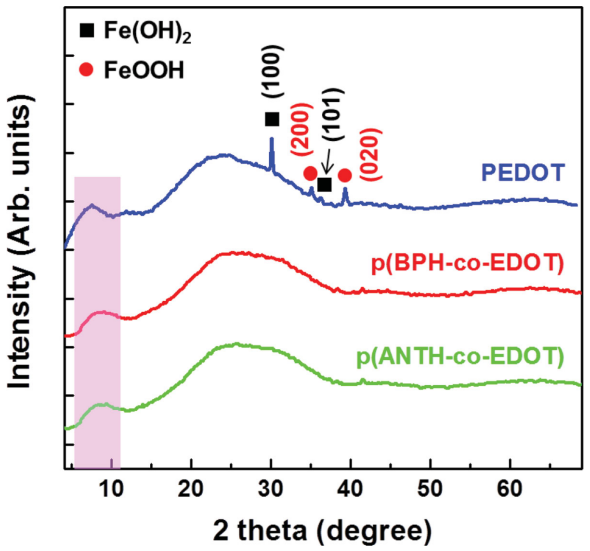

Figure 7. Bragg-Brentano X-ray diffraction patterns of oCVD PEDOT homo- and copolymer films.

technique using EDOT with the incorporation of the crosslinking monomers. p(ANTH-co-EDOT) and p(BPH-co-EDOT) copolymer films yield higher band gaps of ≈2.3 and ≈2.1 eV, respectively than the homopolymer PEDOT band gap of ≈1.8 eV. This increased band gap observed in copolymers accounts for the significant enhancement of optical transmission in the visible regime. Among samples with the film thickness of ≈55 nm, anthracene incorporation leads to the highest transmittance of ≈93%, p(BPH-co-EDOT) of ≈88% and a typical homopolymer PEDOT of ≈80% measured at standard wavelength of 550 nm. Critical degradation of optical transmission in the red edge light wavelengths is generally seen in homopolymer PEDOT and this is a challenging issue. However, oCVD copolymer films show significant improvement. In fact, p(ANTH-co-EDOT) copolymer presents an increase in transmission with increasing wavelength in this regime and reach the transmittance up to ≈99% at 800 nm. The measured electrical conductivity of p(ANTH-co-EDOT) and p(BPH-co-EDOT) is ≈0.5 and ≈30 S cm^{-1}, which is within the semiconducting level and less than that of homopolymer (>1000 S cm^{-1} in general and the highest ≈3500 S cm^{-1} in the present study). Lower doping in copolymers is proved with the analysis of Raman, FTIR and XPS measurements and hence, accounts for the lower conductivity. For the field effect TFT applications as an active channel layer, the channel conductivity modulation with varying carrier density must be achieved by the applications of gate field bias. Copolymer PEDOT with lower doping is much more suitable for the TFT channel applications than heavily doped homopolymer PEDOT since the carrier injection and consequent channel modulation is restricted by the field effect in originally heavily doped materials, consequently, difficult channel modulation. In addition, copolymer PEDOT films are deposited in amorphous state using oCVD which is significantly favorable in flexible and foldable device applications without property degradation due to crack formation compared to brittle materials. Therefore, oCVD-grown amorphous semiconducting PEDOT copolymers with greatly improved optical transmittance may offer a significant opportunity as an active layer in organic optoelectronic device applications such as transparent and flexible thin film transistors.

4. Experimental Section

Preparation of Homopolymer and Copolymer PEDOT Films using oCVD: For the homopolymer PEDOT films, as described elsewhere,[20,52] the precursor vapors of 3,4-ethylenedioxythiophene (EDOT) monomer (Sigma-Aldrich 97%) and oxidizing agent of $FeCl_3$ (Sigma-Aldrich, 99.99%) were delivered into a vacuum chamber to a temperature-controlled stage where they reacted to yield PEDOT films. For the copolymer PEDOT films, additional cross-linking monomers of anthracene ($C_{14}H_{10}$, CAS#120–12–7, Sigma-Aldrich >99%) or biphenyl ($C_{12}H_{10}$, CAS#092–52–4, Sigma-Aldrich 99.5%) were introduced to a chamber along with EDOT monomer and $FeCl_3$. Glass and Si substrates were cleaned with acetone, methanol and de-ionized water, and then fully blow dried substrates were loaded into the oCVD chamber. Prior to all depositions, the oCVD chamber was pumped down to a base pressure of less than 1×10^{-3} Torr by mechanical rotary and molecular turbo pumps connected to the chamber. The depositions were performed at various substrate temperatures ranging 120–170 °C and all as-deposited homo- and copolymer PEDOT films were rinsed with hydrobromic acid (HBr) for 20 min followed by methanol (MeOH) rinse for 20 min to remove residual $FeCl_3$ and unreacted monomers.

Characterizations: Optical transmittance and absorption spectra of oCVD films were collected using a UV–Vis–NIR spectrophotometer (Varian Cary 5000) over wavelengths from 300 to 800 nm. The optical band gap of homopolymer and copolymers can be estimated by extrapolating the linear portion of the curve to wavelength axis and its intercept is determined to the absorption edge wavelength of λ_{ab}.[53] The electrical conductivity was characterized using a four-point probe (Jandel). Raman shift was measured with a Horiba HR800 Raman Confocal Microscope using a 784.399 nm laser. FTIR spectra were obtained on oCVD homo- and copolymer PEDOT films deposited on Si wafers using a Nexus 870 (Thermo Electron Corp.). XPS measurements made on the films on Si were performed with a Surface Science Instruments (SSI) model SSX-100 with operating pressure below 2×10^{-9} Torr using monochromatic Al $K\alpha$ X-rays at 1486.6 eV and photoelectron collecting angle of 55° from the surface normal. The surface topographic images and RMS roughness were obtained using AFM (Veeco Multimode) non-contact height mode. Thicknesses of the films were characterized using a step-height profilometer (Veeco Dektak 150). The Bragg-Brentano coupled-scan XRD patterns to characterize amorphous/crystalline structure and preferred orientation of the materials were carried out in a PANalytical X'Pert Pro diffractometer with $3° < 2\theta < 70°$ using Cu $K\alpha$ radiation ($\lambda = 1.54$ nm) at 45 kV and 40 mA.

Acknowledgements

The authors gratefully acknowledge the financial support of the Eni S.p.A. under the Eni-MIT Alliance Solar Frontiers Program.

Received: August 25, 2014
Revised: September 24, 2014
Published online: October 20, 2014

[1] H. Shirakawa, E. J. Louis, A. G. Macdiarmid, C. K. Chiang, A. J. Heeger, *J. Chem. Soc.-Chem. Commun.* **1977**, 578.
[2] D. Kumar, R. C. Sharma, *Eur. Polym. J.* **1998**, *34*, 1053.
[3] A. Elschner, S. Kirchmeyer, W. Lovenich, U. Merker, K. Reuter, *PEDOT: Principles and Applications of an Intrinsically Conductive Polymer*, Taylor & Francis, New York **2010**.

[4] A. Diaz, *Chem. Scr.* **1981**, *17*, 145.
[5] R. J. Waltman, A. F. Diaz, J. Bargon, *J. Electrochem. Soc.* **1984**, *131*, 1452.
[6] Y. Z. Wang, J. Joo, C. H. Hsu, J. P. Pouget, A. J. Epstein, *Macromolecules* **1994**, *27*, 5871.
[7] R. M. Howden, E. D. McVay, K. K. Gleason, *J. Mater. Chem. A* **2013**, *1*, 1334.
[8] S. A. Spanninga, D. C. Martin, Z. Chen, *J. Phys. Chem. C* **2010**, *114*, 14992.
[9] a) A. Kraft, A. C. Grimsdale, A. B. Holmes, *Angew. Chem. Int. Ed.* **1998**, *37*, 402; b) U. Mitschke, P. Bauerle, *J. Mater. Chem.* **2000**, *10*, 1471.
[10] G. Horowitz, *Adv. Mater.* **1998**, *10*, 365.
[11] C. J. Brabec, N. S. Sariciftci, J. C. Hummelen, *Adv. Funct. Mater.* **2001**, *11*, 15.
[12] M. C. Barr, R. M. Howden, R. R. Lunt, V. Bulovic, K. K. Gleason, *Adv. Energy Mater.* **2012**, *2*, 1404.
[13] R. M. Howden, E. J. Flores, V. Bulovic, K. K. Gleason, *Org. Electron.* **2013**, *14*, 2257.
[14] S. G. Im, K. K. Gleason, E. A. Olivetti, *Appl. Phys. Lett.* **2007**, *90*.
[15] M. C. Barr, J. A. Rowehl, R. R. Lunt, J. Xu, A. Wang, C. M. Boyce, S. G. Im, V. Bulovic, K. K. Gleason, *Adv. Mater.* **2011**, *23*, 3500.
[16] S. G. Im, D. Kusters, W. Choi, S. H. Baxamusa, M. C. M. v. de Sanden, K. K. Gleason, *ACS Nano* **2008**, *2*, 1959.
[17] H. Chelawat, S. Vaddiraju, K. Gleason, *Chem. Mater.* **2010**, *22*, 2864.
[18] S. G. Im, P. J. Yoo, P. T. Hammond, K. K. Gleason, *Adv. Mater.* **2007**, *19*, 2863.
[19] a) D. C. Borrelli, M. C. Barr, V. Bulovic, K. K. Gleason, *Sol. Energy Mater. Sol. Cells* **2012**, *99*, 190; b) D. C. Borrelli, S. Lee, K. K. Gleason, *J. Mater. Chem. C* **2014**, *2*, 7223.
[20] S. G. Im, K. K. Gleason, *Macromolecules* **2007**, *40*, 6552.
[21] D. C. Borrelli, K. K. Gleason, *Macromolecules* **2013**, *46*, 6169.
[22] D. Bhattacharyya, R. Yang, K. K. Gleason, *J. Mater. Chem.* **2012**, *22*, 17147.
[23] S. Vaddiraju, K. K. Gleason, *Nanotechnology* **2010**, 21.
[24] S. Vaddiraju, K. Senecal, K. K. Gleason, *Adv. Funct. Mater.* **2008**, *18*, 1929.
[25] D. Bhattacharyya, K. Senecal, P. Marek, A. Senecal, K. K. Gleason, *Adv. Funct. Mater.* **2011**, *21*, 4328.
[26] H. Park, R. M. Howden, M. C. Barr, V. Bulovic, K. Gleason, J. Kong, *ACS Nano* **2012**, *6*, 6370.
[27] D. Bhattacharyya, K. K. Gleason, *Chem. Mater.* **2011**, *23*, 2600.
[28] J. P. Lock, J. L. Lutkenhaus, N. S. Zacharia, S. G. Im, P. T. Hammond, K. K. Gleason, *Synth. Met.* **2007**, *157*, 894.
[29] M. Fabretto, J. P. Autere, D. Hoglinger, S. Field, P. Murphy, *Thin Solid Films* **2011**, *519*, 2544.
[30] C. J. M. Emmott, A. Urbina, J. Nelson, *Sol. Energy Mater. Sol. Cells* **2012**, *97*, 14.
[31] B. G. Lewis, D. C. Paine, *MRS Bull.* **2000**, *25*, 22.
[32] M.-G. Kang, M.-S. Kim, J. Kim, L. J. Guo, *Adv. Mater.* **2008**, *20*, 4624.
[33] H.-Z. Geng, K. K. Kim, K. P. So, Y. S. Lee, Y. Chang, Y. H. Lee, *J. Am. Chem. Soc.* **2007**, *129*, 7758.
[34] S. Bae, H. Kim, Y. Lee, X. Xu, J.-S. Park, Y. Zheng, J. Balakrishnan, T. Lei, H. R. Kim, Y. I. Song, Y.-J. Kim, K. S. Kim, B. Ozyilmaz, J.-H. Ahn, B. H. Hong, S. Iijima, *Nat. Nanotechnol.* **2010**, *5*, 574.
[35] a) H. Chang, G. Wang, A. Yang, X. Tao, X. Liu, Y. Shen, Z. Zheng, *Adv. Funct. Mater.* **2010**, *20*, 2893; b) C. M. Weber, D. M. Eisele, J. P. Rabe, Y. Liang, X. Feng, L. Zhi, K. Muellen, J. L. Lyon, R. Williams, D. A. V. Bout, K. J. Stevenson, *Small* **2010**, *6*, 184.
[36] B. G. Streetman, S. K. Banerjee, *Solid State Electronic Devices*, Pearson Prentice Hall, New Jersey **2006**.
[37] Y. H. Wijsboom, A. Patra, S. S. Zade, Y. Sheynin, M. Li, L. L. W. Shimon, M. Bendikov, *Angew. Chem. Int. Ed.* **2009**, *48*, 5443.
[38] B. L. Groenendaal, F. Jonas, D. Freitag, H. Pielartzik, J. R. Reynolds, *Adv. Mater.* **2000**, *12*, 481.
[39] Y.-j. Tao, Z.-y. Zhang, X.-q. Xu, Y.-j. Zhou, H.-f. Cheng, W.-w. Zheng, *Electrochim. Acta* **2012**, *77*, 157.
[40] a) G. Vaubel, H. Baessler, *Phys. Lett. A* **1968**, *A27*, 328; b) J. Gascon, M. D. Hernandez-Alonso, A. R. Almeida, G. P. M. van Klink, F. Kapteijn, G. Mul, *ChemSusChem* **2008**, *1*, 981.
[41] E. F. Schubert, *Light-Emitting Diodes*, SPIE – The International Society for Optical Engineering, **2002**.
[42] S. Lee, D. C. Paine, K. K. Gleason, *Adv. Funct. Mater.* **2014**, DOI: 10.1002/adfm.201401282.
[43] a) J. Ouyang, C. W. Chu, F. C. Chen, Q. F. Xu, Y. Yang, *J. Macromol. Sci.- Pure Appl. Chem.* **2004**, *A41*, 1497; b) J. Ouyang, Q. F. Xu, C. W. Chu, Y. Yang, G. Li, J. Shinar, *Polymer* **2004**, *45*, 8443.
[44] F. Tran-Van, S. Garreau, G. Louarn, G. Froyer, C. Chevrot, *J. Mater. Chem.* **2001**, *11*, 1378.
[45] S. Garreau, G. Louarn, J. P. Buisson, G. Froyer, S. Lefrant, *Macromolecules* **1999**, *32*, 6807.
[46] J. P. Lock, S. G. Im, K. K. Gleason, *Macromolecules* **2006**, *39*, 5326.
[47] S. Rattan, P. Singhal, A. L. Verma, *Polym. Eng. Sci.* **2013**, *53*, 2045.
[48] S. V. Selvaganesh, J. Mathiyarasu, K. L. N. Phani, V. Yegnaraman, *Nanoscale Res. Lett.* **2007**, *2*, 546.
[49] a) K. K. Zhuravlev, M. D. McCluskey, *J. Chem. Phys.* **2002**, *117*, 3748; b) M. D. Halls, C. P. Tripp, H. Bernhard Schlegel, *Phys. Chem. Chem. Phys.* **2001**, *3*, 2131.
[50] J. E. Roser, A. Ricca, L. J. Allamandola, *Astrophys. J.* **2014**, *783*, 97.
[51] a) Y. H. Ha, N. Nikolov, S. K. Pollack, J. Mastrangelo, B. D. Martin, R. Shashidhar, *Adv. Funct. Mater.* **2004**, *14*, 615; b) S. Sadki, P. Schottland, N. Brodie, G. Sabouraud, *Chem. Soc. Rev.* **2000**, *29*, 283; c) S. Kirchmeyer, K. Reuter, *J. Mater. Chem.* **2005**, *15*, 2077.
[52] A. M. Coclite, R. M. Howden, D. C. Borrelli, C. D. Petruczok, R. Yang, J. L. Yaguee, A. Ugur, N. Chen, S. Lee, W. J. Jo, A. Liu, X. Wang, K. K. Gleason, *Adv. Mater.* **2013**, *25*, 5392.
[53] a) Q. Zhang, J. Feng, K. Liu, D. Zhu, M. Yang, H. Ye, X. Liu, *Synth. Met.* **2006**, *156*, 804; b) D. Bhattacharyya, K. K. Gleason, *J. Mater. Chem.* **2012**, *22*, 405.